The Surface Wave Environment in the GATE B/C Scale—Phase III

V. CARDONE

Oceanweather, Incorporated, White Plains, NY 10601

H. CARLSON

Deutsches Hydrographisches Institut, 2000 Hamburg 4, Federal Republic of Germany

J. A. EWING

Institute of Oceanographic Sciences, Wormley, Surrey, GU8 5UB, England

K. HASSELMANN

Max Planck Institut fur Meteorologie, Geomaticum, Hamburg, 13, Federal Republic of Germany

S. LAZANOFF

Fleet Numerical Oceanography Center, Monterey, CA 93940

W. McLEISH and D. ROSS

National Oceanic and Atmospheric Administration, Atlantic Oceanographic and Meteorological Laboratories, Sea-Air Interaction Laboratory, Miami, FL 33149

(Manuscript received 22 September 1980, in final form 11 June 1981)

ABSTRACT

The surface wave environment in the GATE B/C scale is described from wave measurements made from buoys and aircraft during Phase III (September 1974). Particular emphasis is given to the wave measurements made from the pitch-roll buoy deployed in the B-scale array from the ship *Gilliss* and a similar buoy deployed in the C-scale array from *Quadra*. Reduction of the pitch-roll buoy measurements provided estimates of the one-dimensional wave spectrum as well as of the mean direction and spread of wave energy as a function of frequency. The data clearly revealed the importance of external forcing on the wave climate in GATE. Most of the wave energy present in the GATE area was found to be swell imported from the trade wind circulations of both hemispheres and from an intense extratropical cyclone which crossed the North Atlantic at high latitudes early in Phase III. Locally generated waves were clearly evident in the wave spectra, but their energy level may have been modulated significantly by the low-frequency swell. The GATE wave data set can provide a powerful test of contemporary numerical wave-prediction models. The present study defines the attributes which are required of such models for meaningful application to the GATE needs.

1. Introduction

The oceanographic subprogram of the GARP Atlantic Tropical Experiment (GATE) included an extensive surface-wave measurement program. That program emphasized, wave measurements from buoys deployed in the C-scale[1] array during Phase III (the period 30 August–19 September 1974) from which frequency spectra and, from some buoys, directional spectra could be estimated. The C-scale measurements were supplemented by measurements from certain B-scale platforms and, on selected days in Phase III, by measurements from aircraft equipped with laser wave profilometers or airborne imaging radar.

The extensive wave data set collected in GATE simultaneously with planetary boundary-layer and upper ocean data is of potentially significant value in the resolution of certain air-sea interaction questions which are quite relevant to some of the central scientific objectives of GATE. For example, how does the surface wave field affect the transfers of momentum, heat, and water vapor across the air-sea interface? How is the air-sea momentum flux

---

[1] Measurement platforms in GATE were arranged in arrays of three scales: A covered the entire tropical Atlantic, B the eastern tropical zone, while C was positioned within the B scale array to study mesoscale systems with dimensions of 10–100 km.

---

partitioned between surface waves and mean current? Must surface waves be accounted for explicitly in the specification of the transfer processes within the upper oceanic mixed layer?

A principal objective of the wave-measurement program was to obtain high-quality data sets so that a definitive evaluation of contemporary numerical spectral ocean-wave prediction models could be made. It was intended that such validation studies would identify critical failings in present models and lead to improvements in the representations of the physical processes governing wave generation, dissipation, interaction and propagation which comprise such models. The processing and exchange of GATE wave data have generally lagged that of most GATE data sets, and studies with joint data sets of the type suggested above have not yet been completed.

The purpose of this paper is to present a general description of the GATE wave-measurement program and the results of analysis of wave data obtained from selected B/C-scale platforms. The small fraction of the total data set analyzed here appears to be sufficient to resolve the general features of the surface-wave environment in Phase III and to identify characteristic properties of the one and two-dimensional wave spectra peculiar to the GATE area. This study also identifies the necessary scope of studies designed to evaluate wave-prediction models and suggests that the GATE wave data will be uniquely valuable in such studies.

2. Wave measurements

Wave measurement systems deployed during Phase III consisted of six telemetering Datawell wave-rider buoys, five tethered pitch-roll buoys developed by the U.K. Institute of Oceanographic Sciences, the Deutsches Hydrographisches Institut and the U.S. National Oceanic and Atmospheric Administration, several hull-mounted pressure/accelerometer systems aboard USSR ships, and two Spectra Physics laser profilometers aboard two U.S. aircraft. The buoy locations are shown in Fig. 1.

Wave-rider buoys at stations 1G–6G in Fig. 1 furnished measurements of the vertical component of acceleration of the water surface from which wave-height spectra were obtained. Pitch-roll buoys at stations H5 and H6 in Fig. 1 also made measurements of the tilt of the water surface, so that the mean direction of wave propagation and the spread in wave direction at each frequency were obtained, also.

Wave-height frequency spectra were calculated from acceleration spectra, S_a by $S(f) = S_a(f)/(2\pi f)^4$ with units of m^2 per cycle per second (m^2 cps^{-1}).
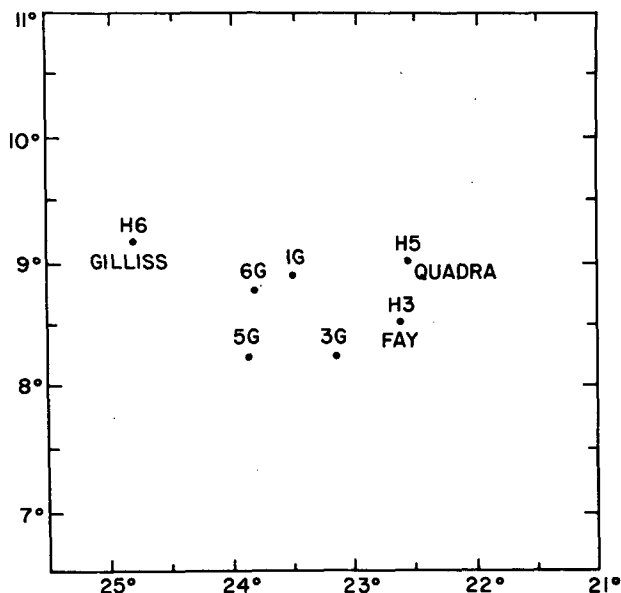
Mean wave directions and directional spread were

FIG. 1. Wave measurement sites in GATE Phase III (H-pitch-roll buoy, G-wave rider).

calculated for each frequency according to Longuet-Higgins et al. (1963).

$$\theta_m(f) = \tan^{-1}[Q13(f)/Q12(f)],$$

$$\theta_s(f) = \left(2 - 2\left\{\frac{Q12^2(f) + Q13^2(f)}{C11(f)[C22(f) + C33(f)]}\right\}^{1/2}\right)^{1/2},$$

where C is the cospectrum, Q is the quadrature spectrum, 1 represents acceleration, 2 refers to the north-south component of tilt, and 3 refers to the east-west component of tilt.

Fig. 2 presents a comparison of one-dimensional spectra obtained by the pitch-roll buoys aboard *Fay* and *Quadra* and a wave rider buoy deployed from *Meteor* (WMO, 1976). A comparison of a laser-profilometer-derived spectrum with that from the pitch-roll buoy aboard *Gilliss* is shown in Fig. 3 (WMO, 1976). The intercomparison data sets suggest that all systems yielded measurements of significant wave height probably accurate to ~10%. Some unknowns exist, however, in the location of spectral peaks in the case of the airborne laser systems since an *a priori* assumption of the direction of the waves is required to map the spectrum observed relative to the aircraft to a fixed coordinate system. The assumption made was that all waves were going in the direction of the wind. Swell systems, therefore, may be incorrectly mapped by laser and the observed spectral peaks may be in error by several frequency bands.

3. Wind-field characteristics

The general meteorological conditions encountered in the GATE have been elaborated in many prior
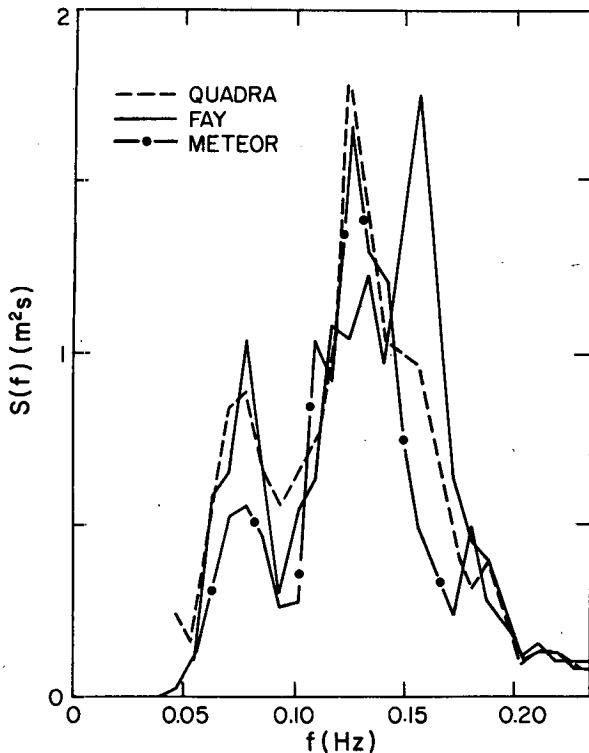
FIG. 2. Intercomparison of wave spectra at 1330 GMT 21 September (*Quadra* and *Fay*-pitch-roll buoys, *Meteor*-wave rider).

studies (e.g., Report of the U.S. GATE Central Program Workshop, 1977). Most such studies have emphasized cloud and precipitation structure in convective systems, the kinematics of the tropospheric wind field as derived from aircraft and sounding data, and the microscale distribution of atmospheric variables within the boundary layer. However, of particular interest for the interpretation of the wave measurements made in GATE is the surface wind field over the GATE area during Phase III, especially for the period between 10 and 14 September, for which many directional spectra from both *Gilliss* and *Quadra* sites were analyzed. The surface streamline analyses prepared for the A-scale, West Africa and adjacent areas, at six-hourly intervals at Dakar, and archived on microfilm as part of the GATE preliminary data set, provide a very general picture of the surface wind. Krishnamurti and Krishnamurti (1978) applied objective analysis techniques to produce A-scale wind fields at 12 h intervals for the surface and 850 mb levels for the 100-day GATE period. Sadler and Oda (1978) applied manual kinematic-analysis techniques to describe once daily the surface and 250 mb wind fields over the A scale.

In this study, the Dakar A-scale charts for the period 10–14 September were reanalyzed so that streamlines and isotachs of the effective 19.5 m level wind were available for the area bounded by 5°N,

20°N, 5°W and 35°W. The calculation of the effective 19.5 m wind, described originally by Cardone (1969), involves first the calculation of the wind stress for each observation from the anemometer height and the measured wind speed, air temperature and humidity, and sea temperature. Standard similarity wind-profile forms are coupled with a roughness-parameter representation which is an interpolation between that for aerodynamically smooth flow at low stress and the Charnock-law form proposed recently by Garratt (1977). Moisture stratification was included in the estimation of the stability length. The effective 19.5 m wind is then the wind speed at a height of 19.5 m that is consistent with the calculated stress in a neutral atmosphere for the assumed wind-profile model. This procedure tends to remove the variability in isotach analyses and in wind-wave relationships which might be introduced by variable stability or measurement height within a data set.

Fig. 4 is an example of the reanalyzed A-scale streamline/isotach charts. The most significant features of the wind analysis are:

1) The northeast trade winds of speeds 6–8 m s^{-1}, which extend south to 15°N.

2) The Intertropical Convergence Zone (ITCZ), which is characterized by generally weaker winds, cols and aymptotes in the streamline pattern, and several closed circulations, one of which in the C-scale is accompanied by winds up to 8 m s^{-1}.

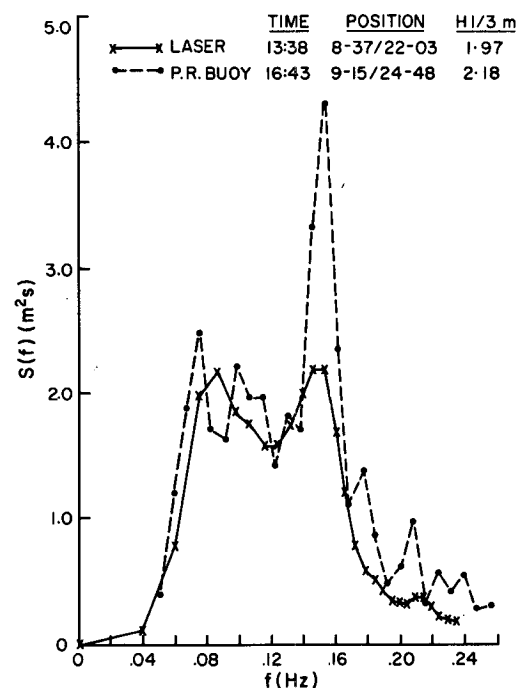3) The cross-equatorial flow, or southwest mon-

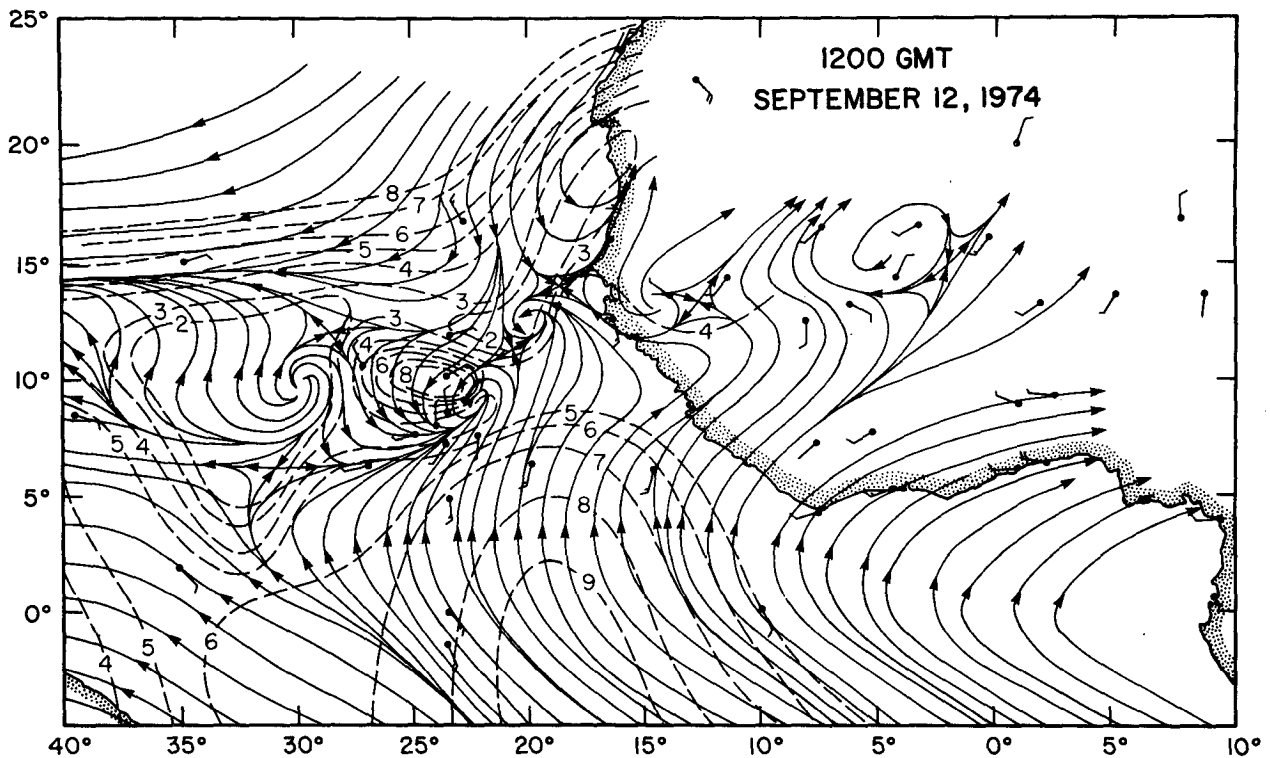FIG. 3. Comparison of wave spectra from laser and from pitch-roll buoy, 8 September.

FIG. 4. Streamline and isotach analysis of GATE A-scale surface wind field. Wind speeds are in m s.$^{-1}$

soonal surface flow near Africa with a speed of 5 m s^{-1}.

4) The northern extent of the South Atlantic southeast trades with speeds up to 9 m s^{-1}.

Toward the middle of September the cross-equatorial flow strengthened gradually and spread northward so that by 14 September the entire B/C-scale was within the southerly flow of speeds up to 11 m s^{-1}.

The reanalyzed A-scale charts were gridded (speed and direction) at 1° latitude/longitude intersections for future use in wave hindcast studies. After the digitization, type 1 ship data became available on tape. The wind observations in type 1 data represent hourly averages computed from automatic-recording-buoy or boom-mounted wind sensors. Type 1 data were not used in the A-scale analysis, and it is therefore interesting to compare these withheld data to the gridded A-scale winds. Fig. 5 compares the grid winds with winds recorded from the *Meteor* buoy. While the winds compare favorably, smaller scale structures are missed in the A-scale analyses, especially on 13 and 14 September. To resolve small-scale systems, both to aid in the interpretation of the wave data and to use in future hindcast studies, a reanalysis of the surface wind field was performed over the region 5–12°N, 20–27°W using only the type 1 wind data, again converted to effective 19.5 m winds. Analyses

were prepared at 3 h intervals for 13 and 14 September only, and were digitized at 0.5° latitude-longitude intersections. A typical example of the high-resolution analyses is shown in Fig. 6, which applies to 2100 GMT 13 September. Interesting features of this particular analysis include 1) the strong cross-equatorial flow with speeds (effective) of 12 m s^{-1}; 2) the small scales present in the surface wind field over the B/C scale, at a time when the ITCZ is shifting temporarily northward; and 3) the small vortex, which had been tracked westward from the 12th and which has just passed *Gilliss*.

Surface wind fields were not produced for extra-tropical regions outside the GATE A-scale. However, for selected wave "events" observed in the GATE area that involved swell, the associated wind-field characteristics in subtropical and high-latitude weather systems in the North Atlantic Ocean were assessed using standard synoptic ship-report data, analyzed Northern Hemisphere sea level pressure analyses, and the daily kinematic analyses prepared by Sadler and Oda.

4. General properties of the wave measurements

Directional wave measurements were available from the pitch-roll buoys at *Gilliss*, *Quadra* and *Fay* daily through most of Phase III. The time histories of significant wave height from the *Gilliss* and
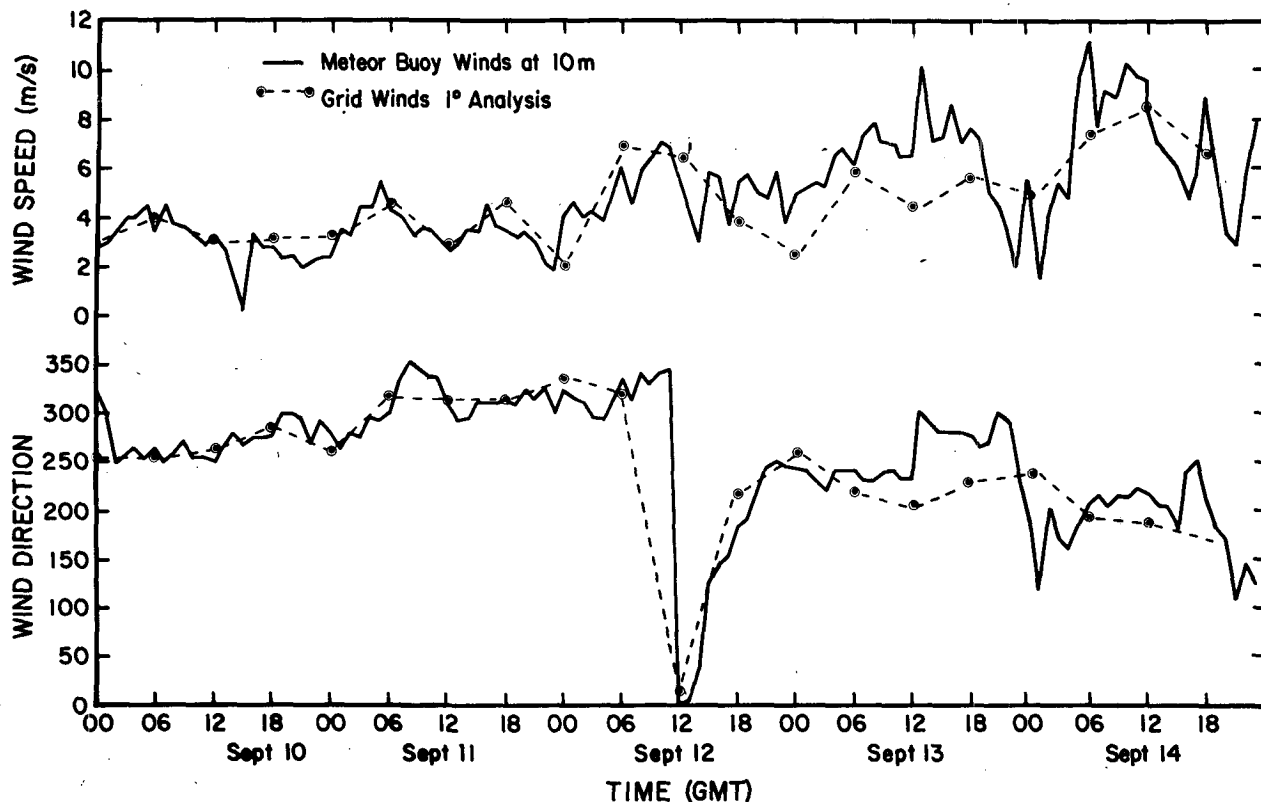
FIG. 5. Comparison of wind speeds at *Meteor* from digitized 1° A-scale analysis and from hourly averages of observations.
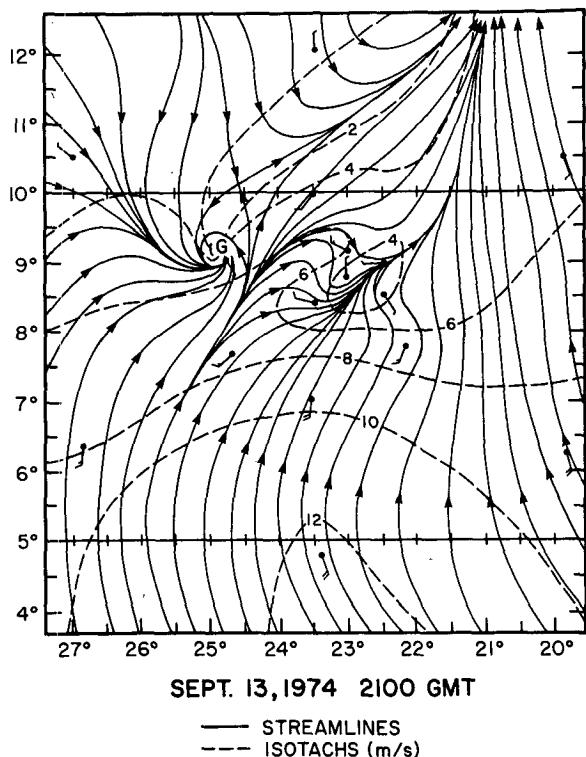

SEPT. 13, 1974 2100 GMT

——— STREAMLINES
– – – ISOTACHS (m/s)

FIG. 6. High-resolution streamline and isotach analysis of surface winds (G—location of *Gilliss*). Wind speeds are in m s.$^{-1}$

Quadra sites are shown in Fig. 7 along with the time histories of surface wind speed at *Gilliss* for the period 3–18 September. Significant wave heights never decreased below about 1.4 m and averaged 1.92 (±0.24) m at *Gilliss*, 1.85 (±0.29) m at *Quadra* and 1.82 (±0.26) m at *Fay*. There is little correlation between the wave height and wind-speed time series at *Gilliss*, even if the expected lag of the waves behind the wind is considered. Increases in significant wave height to above 2 m occurred at *Gilliss* on the 5th, 7th, 9th, 13th, 14th and 17th, but only the increase on the 7th appears to be related to increasing winds in the B/C-scale area. The increased surface wind on that day resulted from a surge in the southwest cross-equatorial flow which began early on the 6th. In general, the wave heights are two to three times higher than fully developed seas (Pierson and Moskowitz, 1964) at the wind speeds encountered. This suggests that most of the wave energy present in the GATE area was swell.

This is verified by a typical directional spectrum such as analyzed for a *Gilliss* pitch-roll buoy record taken on 8 September, as shown in Fig. 8, which shows the properties of the wave spectra characteristic of the GATE wave data. The one-dimensional spectrum shows two important regions of wave energy, one centered at 0.094 Hz, the sec-
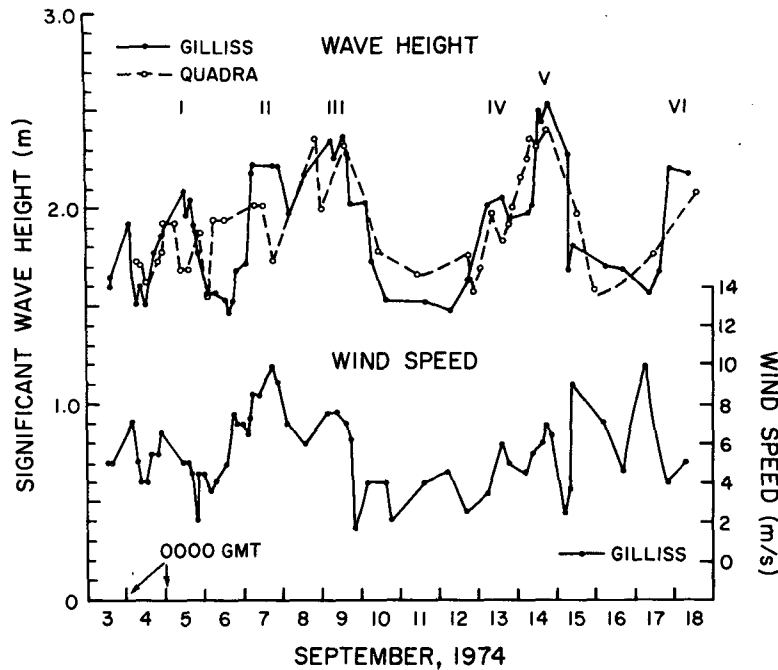
FIG. 7. Comparison of significant wave heights with wind speeds. Roman numerals denote periods of increased wave heights.

ond at 0.172 Hz. Spectral components at frequencies near and above 0.172 Hz are directed about the local wind direction, while the low-frequency energy is associated with waves propagating nearly 90° from the wind direction. There is a characteristic sharp falloff in energy to the right of the apparent wind-wave peak frequency, while beyond about twice the peak wind-wave frequency the spectrum falls off as f^{-5} until about 0.65 Hz, at which limitations of the buoy response become effective. The range of f^{-5} behavior can be found in the plot of normalized one-dimensional energy $S_n(f)$, where $S_n(f) = S(f)f^5$ $(2\pi)^4/g^2$. The equilibrium range constant α is estimated as the average value of $S_n(f)$ over the range of frequencies in which $S_n(f)$ is essentially constant. The spreading of wave energy was found to be at a minimum at the wind-sea peak frequency, a result in agreement with the spreading function proposed by Mitsuyasu *et al.* (1975).

The meteorological conditions over the B/C scale on the 8th favored the active generation of wind waves. For 24 h prior to the time of the wave record represented in Fig. 8, wind speeds ranged between 8 and 10 m s^{-1} with practically constant direction. Nevertheless, the spectrum shown in Fig. 8 shows considerable energy at frequencies below the wind-wave frequencies. The swell energy is propagating toward the northwest, which is suggestive of a source generating zone in the southeast trades below the equator (see, e.g., the wind field for a different date in Fig. 4).

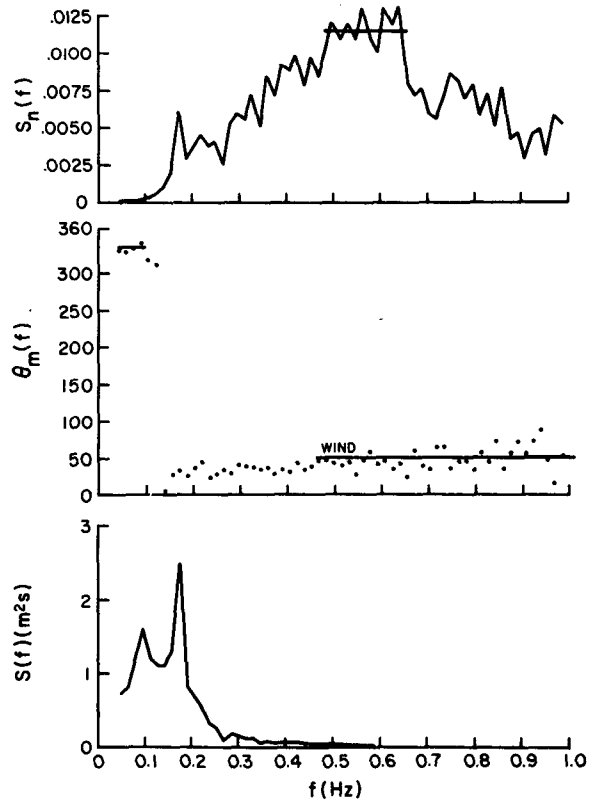Many spectra exhibited *two* distinct regions of

FIG. 8. Directional wave analysis from *Gilliss*, 0327 GMT 8 September. Two peaks in the wave-height spectrum have different mean directions, one parallel to the wind. A determination of α is illustrated, the large apparent jump in wave direction is caused by a break in the azimuth scale at 360°.

TABLE 1. Wave properties at *Gilliss*.

Date	Time (GMT)	$\bar{V}$	θ_v	$\delta_{pm}{}^2$	f_{pm}	δ^2	$\bar{H}^{1/3}$	f_1	θ_1	f_2	θ_2	α_w	ϵ	$\epsilon. \times 10^3$
9/3	1515	5.0	220	0.031	0.239	0.160	1.60	0.125	253			0.0057	0.0144	6.91
9/3	1546	5.0	220	0.031	0.239	0.168	1.64	0.109	313	0.141	281	0.0053	0.0150	7.19
9/4	0246	7.0	290	0.109	0.175	0.232	1.93	0.125	223			0.0078	0.0059	2.83
9/4	0731	5.0	290	0.031	0.239	0.144	1.52	0.109	211			0.0034	0.0129	6.12
9/4	0914	.4.0	290	0.013	0.298	0.162	1.61	0.109	203			0.0048	0.0347	1.66
9/4	1052	4.0	310	0.013	0.298	0.140	1.50	0.109	206			0.0044	0.0220	10.5
9/4	1400	5.5	285	0.046	0.217	0.166	1.63	0.125	215			0.0050	0.0100	4.79
9/4	1727	5.5	330	0.046	0.217	0.198	1.78	0.125	248			0.0052	0.0120	5.75
9/4	1943	6.5	280	0.081	0.188	0.195	1.77	0.125	233			0.0056	0.0067	3.21
9/4	2225	7.5	280	0.134	0.166	0.216	1.86	0.125	241			0.0069	0.0045	2.16
9/5	1118	5.0	340	0.031	0.239	0.278	2.11	0.125	240			0.0090	.0250˙	11.9
9/5	1158	5.0	340	0.031	0.239	0.240	1.96	0.125	228			0.0078	0.0216	10.4
9/5	1617	m	m	m	m	0.262	2.05	0.109	231	0.172	159	a	m	
9/5	1652	4.5	160	0.021	0.265	0.226	1.90	0.125	235	0.188	133	a	0.0300	14.4
9/5	1900	4.5	190	0.021	0.265	0.221	1.88	0.125	229	0.188	120	0.0056	0.0293	14.0
9/5	2204	2.0	240	0.001	0.571	0.194	1.76	0.109	219	0.188	99	0.0030	0.5403	258.9
9/5	2250	4.5	240	0.021	0.265	0.196	1.77	0.109	251	0.14	206	0.0036	0.0260	12.4
9/6	0320	3.5	260	0.009	0.327	0.156	1.50	0.094	221			0.0048	0.0483	23.1
9/6	0732	4.0	260	0.013	0.298	0.156	1.58	0.125	266			0.0047	0.0334	16.1
9/6	1458	5.0	260	0.031	0.239	0.144	1.52	0.109	241			0.0057	0.0129	6.19
9/6	1539	7.5	205	0.134	0.166	0.137	1.48	0.109	236			0.0061	0.0028	1.34
9/6	1619	7.0	240	0.109	0.175	0.146	1.53	0.109	225			0.0054	0.0037	1.78
9/6	2252	7.0	240	0.109	0.175	0.178	1.68	0.125	263			0.0073	0.0045	2.16
9/7	0218	6.5	230	0.081	0.188	0.185	1.72	0.125	255			0.0084	0.0064	3.07
9/7	0732	8.5	225	0.222	0.147	0.300	2.19	0.125	242	0.172	33	0.0072	0.0037	1.77
9/7	0806	8.5	225	0.222	0.147	0.308	2.22	0.141	312	0.172	49	0.0084	0.0039	1.87
9/7	1931	10.0	220	0.424	0.124	0.302	2.2	0.156	40			0.0080	0.0020	.960
9/7	2227	9.0	210	0.278	0.138	0.294	2.17	0.094	310	0.156	27	0.0087	0.0029	1.39
9/8	0322	7.0	220	0.109	0.175	0.245	1.98	0.094	342	0.172	34	0.0105	0.0063	3.02
9/8	1643	6.0	210	0.059	0.204	0.297	2.18	0.078	338	0.156	12	0.0071	0.0140	2.39
9/9	0739	7.5	260	0.134	0.166	0.348	2.36	0.078	338	0.125	359	0.0082	0.0072	3.45
9/9	1038	7.5	270	0.134	0.166	0.319	2.26	0.078	348	0.141	27	0.0065	0.0066	2.64
9/9	1440	7.0	270	0.109	0.175	0.357	2.39	0.078	360	0.141	45	0.0076	0.0091	4.36
9/9	1527	6.0	270	0.059	0.204	0.319	2.26	0.078	2	0.141	40	0.0063	0.0151	7.24
9/9	2205	1.5	220	0.0003	0.762	0.255	2.02	0.078	345	0.141	33	a		
9/10	0316	4.0	250	0.013	0.298	0.257	2.03	0.078	339	0.141	27	0.0042	0.0550	26.4
9/10	1515	4.0	305	0.013	0.298	0.185	1.72	0.078	351	0.125	337	0.0048	0.0396	18.9
9/10	1945	2.0	310	0.001	0.571	0.146	1.53	0.078	005	0.156	29	0.0024	0.4066	195
9/11	1650	4.0	330	0.013	0.298	0.144	1.52	0.078	359	0.109	334	0.0044	0.0308	14.7
9/12	0845	4.5	330	0.021	0.265	0.137	1.48	0.078	103	0.141	264	0.0063	0.0181	8.68
9/12	1929	2.5	305	0.002	0.457	0.164	1.62	0.078	020	0.141	321	0.0027	0.2284	109.5
9/13	0842	3.5	350	.0.009	0.327	0.257	2.03	0.063	159	0.156	302	0.0056	0.0795	38.1
9/13	1429	6.0	210	0.059	0.204	0.263	2.05	0.063	154	0.172·	298	0.0082	0.0124	5.95
9/13	1921	5.0	151	0.031	.0.239	0.238	1.95	0.078	142	0.141	297	0.0058	0.0214	10.3
9/14	0900	4.5	165	0.021	0.265	0.242	1.97	0.078	159	0.125	319	0.0055	0.0321	15.4
9/14	1056	5.5	160	0.046	0.217	0.265	2.06	0.078	160	0.141	315	0.0056	0.0160	7.67
9/14	1334	6.0	190	0.059	0.204	0.394	2.51	0.078	188	0.125	003	0.0058	0.0186	8.92
9/14	1528	7.0	205	0.109	0.175	0.375	2.46	0.078	189	0.125	353	0.0074	0.0096	4.6
9/14	1914	6.5	185	0.081	0.188	0.397	2.52	0.078	165	0.125	004	0.0082	.0136	6.52
9/15	0841	2.5	180	0.002	0.457	0.328	2.29	0.078	174	0.141	015	0.0047	0.4567	219
9/15	0956	3.5	205	0.009	0.327	0.176	1.68	0.109	196	0.141	349	0.0065	0.0546	26.2
9/15	1036	9.0	190	0.279	0.139	0.205	1.81	0.125	226			0.0072	0.0023	0.96
9/16	1541	7.0	240	0.109	0.175	0.181	1.70	0.109	167			0.0062	0.0046	2.2
9/16	1923	4.5	200	0.021	0.265	0.178	1.69	0.109	218	0.141	329	0.0070	0.0236	11.3
9/17	0910	10.0	330	0.424	0.124	0.154	1.57	0.125	289			0.0066	0.0010	0.479
9/17	1431	m	30	m	m	0.176	1.68	0.094	241	0.125	013	a	m	
9/17	2126	4.0	225	.013	0.298	0.305	2.21	0.094	243				0.0654	31.4
9/18	1034	5.0	170	0.031	0.239	0.300	2.19	0.094	248			a	0.0269	12.9

Explanation of Table:

$\bar{V}$ mean wind speed (m s⁻¹)·as measured at 8.2 m
θ_v mean wind direction (°) (from which)
$\delta_{pm}{}^2$ variance of fully developed sea at $V_{19.5}$
f_{pm} peak frequency of fully developed sea at $V_{19.5}$
δ^2 *measured total variance*
f_1 first peak frequency
θ_1 mean wave direction at f_1 (toward which, clockwise from north)
f_2 second peak frequency if present
θ_2 mean wave direction at f_2 (toward which, clockwise from north)
α_w mean value of equilibrium-range constant over wind-wave region of spectrum exhibiting f^{-5} slope, if present
ϵ nondimensional total energy $= \delta^3 g^2 / \bar{V}_{19.5}$
$\epsilon.$ nondimensional total energy $= \delta^2 g / U.^2$
a no apparent f^{-5} region
m missing data

swell energy in addition to high-frequency waves apparently in equilibrium with the local wind. In Table 1 we have listed the properties of all spectra calculated from the pitch-roll measurements made at the *Gilliss*. The total variance and peak frequency are listed, except when two or more relative maxima were clearly evident in the one-dimensional spectra. For those spectra, the two lower-frequency "peak" frequencies, f_1 and f_2, are listed along with their respective mean wave directions θ_1 and θ_2. In many spectra, though wind waves were obviously present, the relative wind-sea peak frequency was masked by the high energy level of swell. Table 1 also includes windspeed and direction measured at the time of the wave measurement and the total variance δ_{pm}^2 and peak frequency f_{pm} computed for the indicated wind speed on the basis of the Pierson-Moskowitz form. In all but a few spectra, the sea states in the GATE area were "overdeveloped" in the sense that the energy levels and wave periods present exceeded considerably those expected from local wind considerations. In view of the considerable swell and the presence of at least two peaks in the spectrum whose location in frequency depended mainly upon the distance from the source region and the characteristics of the wind field therein, it would be pointless to compare the spectral *shapes* in the GATE spectra with simple parametric forms (e.g., the Pierson-Moskowitz or JONSWAP spectra) developed for pure wind-generated seas. Clearly, the wave environment in GATE was dominated by swell. The directional information helped to identify the source of the swell energy, and results of swell studies will be presented in the next section.

Table 1 includes the equilibrium-range constants estimated from those spectra which exhibited a high-frequency range over which $S_n(f)$ was approximately constant and wave directions were within $\pm 20°$ of the local wind direction (see, e.g., Fig. 8). Values could be estimated for all but six out of 58 records at *Gilliss*. The average value of α found was

0.0061, which is ~75% the nominal value of 0.0081 usually quoted.

Phillips (1958) suggested on the basis of dimensional considerations that α should be a universal constant. His argument was based, however, on the assumption that the equilibrium range was governed by wave breaking. The results of the JONSWAP experiment suggest that α is not a constant and that the equilibrium-range behavior is determined by the balance of several processes including wind-wave energy transfer, breaking and nonlinear wave-wave interactions. JONSWAP and other recent studies have suggested that α decreases with fetch x and that a similarity scaling by nondimensional fetch $\xi = gx/U^2$ describes the α variation. Toba (1978), on the other hand, has proposed that there is an explicit dependence of the equilibrium range on local wind speed. The behavior of high-frequency waves in the presence of swell has been treated by Phillips and Banner (1975) who showed that long waves can reduce the maximum amplitude that short waves reach at the point of breaking, as the long waves augment the surface drift near their crests. Kitaigorodskii *et al.* (1975) discussed the convective effects of long waves on short waves under the assumption that a Phillips-type equilibrium range describes the high-frequency wavenumber spectrum. The effect is usually too small to be significant. Mitsuyasu (1977), however, finds high values of α (~0.016) for short fetch conditions in the presence of substantial swell.

The mechanism responsible for the low values of α measured in GATE is not entirely clear. Wind speeds in GATE tended to be lower than in previous studies, and they also were quite variable. A high correlation (~0.9) was found between α and the local wind speed averaged over a 3 h period centered on the wave sampling period. The low energy levels overall are consistent qualitatively with the mechanisms proposed by Phillips and Banner. Phillips (1977) has quantified that effect in terms of the rms slope of the longer waves. For
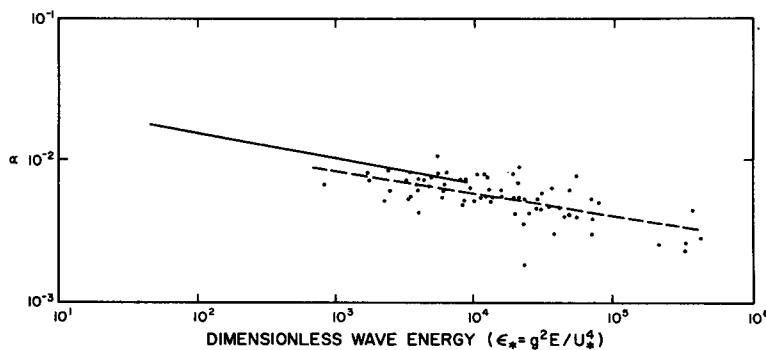

FIG. 9. Log α vs log ϵ_*. A fit to the present values (dashed line) is close to a fit to the values previously assembled by Resio and Vincent (solid line) but the range of ϵ_* is extended by about one order of magnitude.
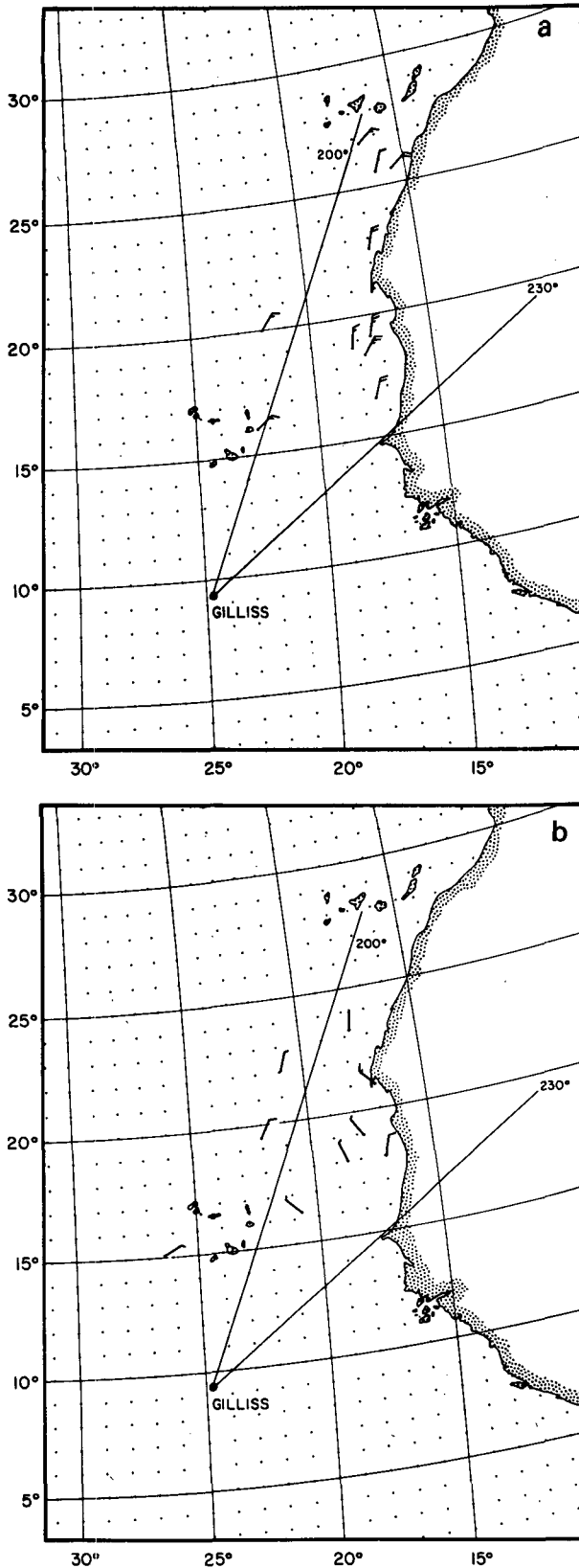
FIG. 10. Winds that could generate southwest swell at *Gilliss*: (a) 2–5 September; (b) 7–10 September. The fetch zone for 200–230° waves is marked.

typical slopes of the swell observed in GATE, the effect should only give a reduction of ~4% in α, which is much smaller than the reductions observed.

On the basis of the energy balance of a wind sea, Hasselmann *et al*. (1976) propose a universal relationship between α and the nondimensional peak frequency $\nu \equiv U f_m/g$, or alternatively the nondimensional total energy $\epsilon \equiv g^2 E/U^4$, where E is total wind-sea variance (or $\epsilon_* \equiv g^2 E/U_*^4$, where U_* is friction velocity). Resio and Vincent (1977) have suggested that α is, in the general case, more appropriately scaled by ϵ_*, with E defined as total variance regardless of its partition between sea and swell. In Fig. 9, we have plotted the GATE data and drawn a fit line to the α values assembled by Resio and Vincent. Despite the considerable scatter, the GATE data tend to confirm the trend in precedent data for α to decrease at large ϵ_*. Within the GATE data, however, the trend in α versus ϵ_* is determined principally by the aforementioned local windspeed dependence.

In nearly all of the directional spectra form GATE Phase III, more than 90% of the wave-height variance resulted from one or more groups of swell. When E is calculated from the wind-wave portions of spectra remaining after the contribution from swell is removed, the data points in Fig. 9 are moved to the left a distance corresponding approximately to one logarithm unit. The new data points lie on the average <70% as high as the fitted line derived from the previous compilation by Resio and Vincent. Thus, the inclusion of swell in the calculation of E causes the α values to fit previous data, but why this is so is not clear.

Another consequence of the rich swell content of waves in the GATE area is the relative homogeneity of the distribution of sea states measured over the wave array despite the large mesoscale variability typical of the wind fields over the B/C-scale, as typified by the wind distribution at 2100 GMT 13 September shown in Fig. 6. One-dimensional spectra estimated from wave measurements from pitch-roll buoy and wave-rider buoys made within about 90 min of the above map hour are remarkably similar.

5. Directional wave characteristics

As noted in the previous section, Phase III could be characterized by six periods during which the significant wave height increased above 2 m. Only the event on the 7th could be related to an increase in energy in the wind-wave part of the spectrum in response to increases in the local wind. In this section we combine the directional wave measurements at *Gilliss* and *Quadra* with the appropriate meteorological evidence to provide a qualitative explanation of each event. Our objectives here are threefold:
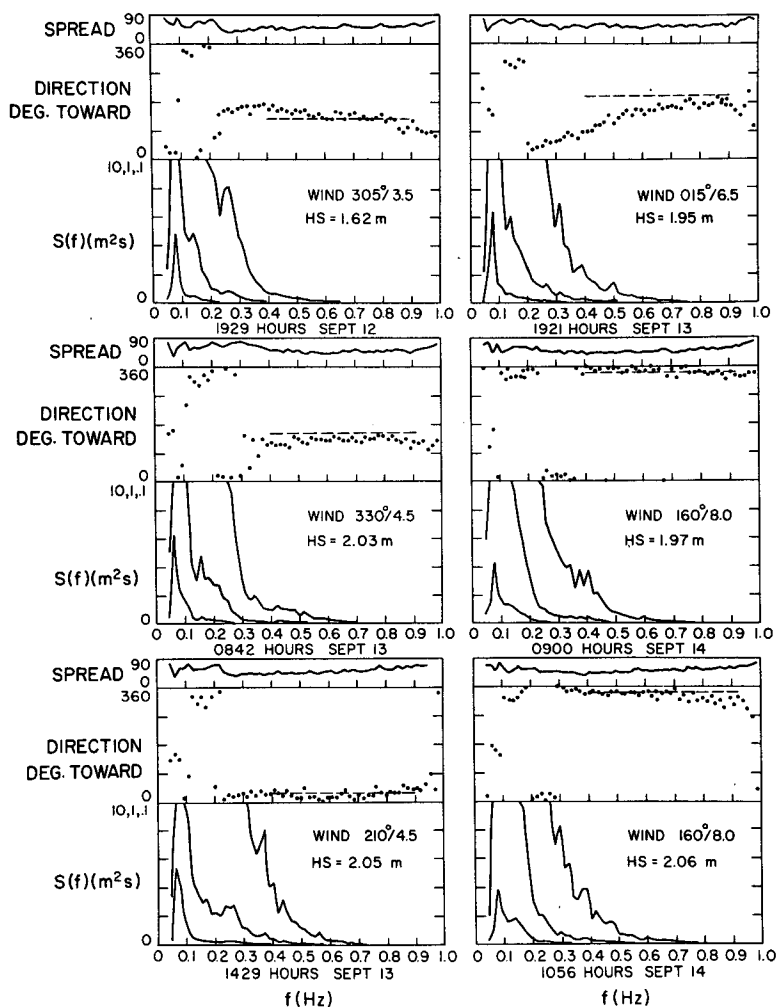
FIG. 11. Directional wave analyses from *Gilliss*, September 12–14. Curves for each analysis are: the directional spread and mean wave direction, as functions of frequency, the one-dimensional spectrum (in three curves corresponding to three scales on ordinate) and a dashed horizontal line to represent the local wind direction.

1) To help establish the validity of the directional wave measurements themselves.

2) To identify the influences on the wave climate in the GATE area in Phase III.

3) To define the context of numerical spectral wave-prediction models required if such models are to be applied at all successfully to the GATE area for comparison with the GATE wave-data set.

The increases in wave height observed on 5 and 17 September were similar in that each was associated with an increase in energy of wave components with frequencies between 0.094 and 0.125 Hz, with mean wave direction generally toward the southwest (210–240°). The energy could not be explained by the winds within the B/C-scale areas as the wind analyses on both of the days showed decreasing winds quite variable in direction. The southwesterly swell in the earlier event was detectable in the

measurements made as early as 3 September and was evident on every wave analysis until 7 September (see Table 1). The mean directions observed suggest a generation source near the northwest African coast north of 15°N. The frequency content of the swell suggests a travel time of one to two days (group velocity 300 n mi day^{-1}) from the general area of suspected generation. To assess the wind-field characteristics in that area, ship reports of wind were composited for the period 2–5 September, a period of suspected active generation (Fig. 10a) and the period 7–10 September when generation should have diminished (Fig. 10b). The former period was characterized by northeasterly winds of 15–25 kt from the vicinity of the Canary Islands as far south as the Cape Verde Islands. Those speeds are sufficiently high to have generated waves with the periods observed. Synoptic sea level pressure charts of the North Atlantic showed the
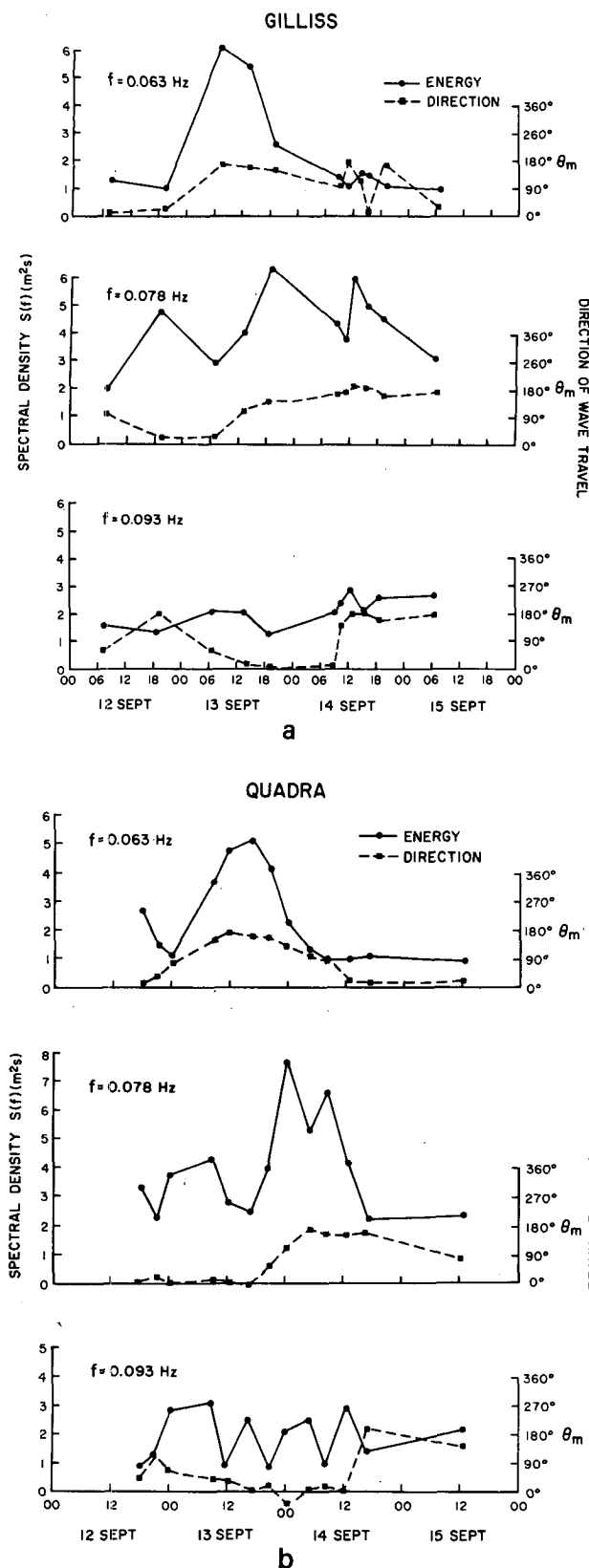
FIG. 12. Spectrum density of swell at three frequencies versus time: (a) *Gilliss*; (b) *Quadra*.

subtropical high pressure system weakening beginning 6 September, and surface winds along the African coast slackened thereafter. Between 7 and 10 September the winds are evidently weak and directed mainly toward the coast. The reappearance of southwesterly swell with frequency near 0.094 Hz at *Gilliss* on the 17th followed the reestablishment of the northeast trades north of 15°N.

The increase in wave height observed on 8 and 9 September was associated with the appearance of swell directed toward the north-northwest (330–360°) with energy concentrated mainly near 0.078 Hz. The swell energy increased through the 8th and peaked on the 1440 GMT wave measurement when the significant wave height reached 2.4 m. The frequency spectrum was double-peaked through this period with the wind-sea peak frequency well separated from the swell peak (see Fig. 8 and Table 1). Through the 9th and the 10th, the swell peak dominated the one-dimensional spectrum, despite the presence of a well-developed wind sea generated by brisk, steady southwest winds. The source of this swell was not studied in detail because of the difficulties in constructing surface wind fields for the South Atlantic Ocean. One possible source is a migratory extratropical cyclone crossing the high-latitude Southern Ocean. Snodgrass et al. (1966) have detected swell in the North Pacific Ocean emanating from such systems in the South Pacific. Cartwright et al. (1978) have recently analyzed wave measurements from St. Helena Island and attributed some of the swell occurrences to storms in the Atlantic sector of the Southern Ocean. In such cases, the great circle paths approach the island from the southwest, and a similar approach direction should be expected in the GATE area for energy from such systems. The source of the swell energy arriving from the southeast at *Gilliss* and *Quadra* is more likely the southeast trade wind core located northeast of the South Atlantic subtropical high. During GATE the core of the southeast trades apparently extended to the southern edge of the A-scale between 15° and 25°W (cf. Figs. 4 and 6) where winds up to 12 m s^{-1} were measured occasionally. Wind speeds could have been even higher farther southeast.

All directional wave analyses performed on the *Gilliss* wave records obtained from 1929 GMT on the 12th to 1056 on the 14th are displayed in Fig. 11. Wave groups at different frequencies present at one time are distinguished by maxima of wave spectra, by different mean directions, and by minima of directional spread. Several noteworthy features of the wave environment in GATE are shown in that figure. First, between 1929 GMT on the 12th and 1429 GMT on the 13th, the low-frequency ($f \sim 0.10$ Hz) swell peak associated earlier with mean wave directions towards the north is replaced by swell propagat-
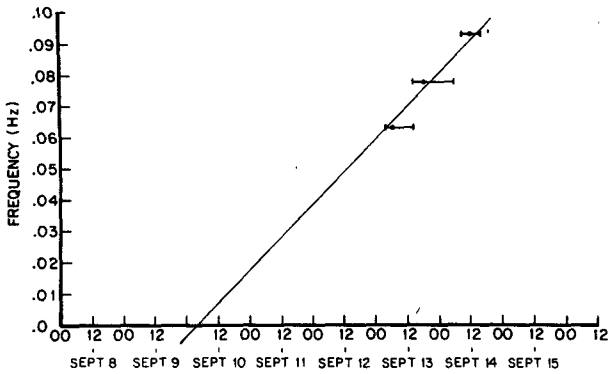
FIG. 13. Swell frequency versus arrival time at *Gilliss*.

ing toward the south-southeast. Meanwhile, the frequency range 0.1–0.2 Hz remains dominated by wave energy that occasionally supports a secondary peak in the one-dimensional spectrum, propagating toward the north-northwest (330–350°). This secondary swell is most likely coming from the same generation source as the lower frequency swell observed between the 7th and 11th.

During the period shown in Fig. 11, wind waves are clearly detectable in the range of frequencies above 0.2 Hz where mean wave directions generally match the local wind direction. The response of the mean high-frequency wave direction to a rapidly turning wind field associated with the passage of a small vortex past *Gilliss* is seen in the sequence of plots between 0642 on the 13th and 0900 on the 14th. While the mean wave direction for waves at the high frequencies indicated tends to track the local wind direction, the spectrum at 1921 on the 13th captures the adjustment process itself, in which only the highest frequency waves ($f \sim 0.6$ Hz) are adjusted, while the response of the lower frequency wind waves lags. The response of the directional wave spectrum to a rapidly turning wind is poorly understood and crudely parameterized in present wave-specification models. The particular sequence of spectra shown in Fig. 11 may be used to test directional response algorithms incorporated in present models and may lead to a better understanding of the adjustment process itself in terms of the details of the spectral energy balance.

As noted above, wave components with frequencies below 0.1 Hz were detected arriving *from* the north-northwest between 12 and 14 September. In Fig. 11, swell energy is seen to dominate the one-dimensional spectrum on the 13th and 14th and to be mainly responsible for the higher wave heights observed on those days. To locate the source of the energy, we plotted time histories of spectral density and mean direction for the spectral bands centered at 0.063, 0.078 and 0.093 Hz. The histories are shown in Fig. 12a for *Gilliss* and Fig. 12b for *Quadra*. More frequent wave measurements are obviously required to resolve the details of the time histories. Nevertheless, there is a remarkable degree of agreement on the characteristics of swell measured at these two stations, indicating both the homogeneity of the swell and the reliability of the pitch-roll systems from *Quadra* and *Gilliss*. The
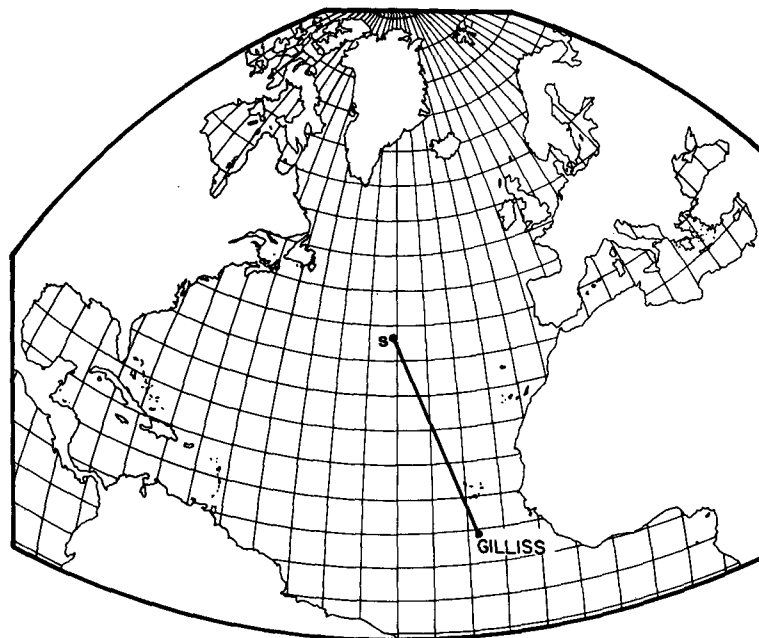

FIG. 14. Deduced location of origin of swell arriving at *Gilliss* September 12–14 on great-circle plot.
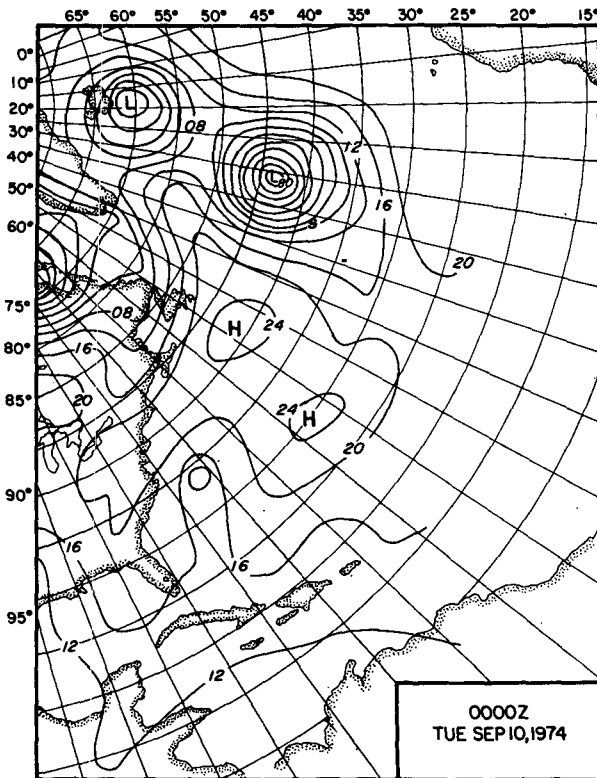
FIG. 15. Surface pressure analysis over North Atlantic Ocean.

histories reveal the pattern expected of well-dispersed swell arriving from a distant generation source. That is, the energy concentrated in the directional bands of interest appears first at the lowest frequency, peaks and then decreases as the adjacent higher frequencies, in turn, experience maximum energy.

In Fig. 13 we have plotted for *Gilliss* the time at each frequency when maximum energy was indicated, on a frequency-time plot. The uncertainty in timing is caused by the coarse temporal resolution in the *Gilliss* wave measurements. Using ridge-line analysis techniques (cf. Snodgrass *et al.*, 1966) the slope and intercept of a line drawn subjectively through the time points defined the distance and time of occurrence of the source of the swell. Next, we used the mean wave direction (168°) averaged over the three maxima in energy to define a great circle through the wave-measurement site as the most likely direction of swell propagation. The deduced source point is shown in Fig. 14. In Fig. 15, the point is seen to lie precisely at the downwind end of an obvious fetch zone trailing an intense cyclone near 45°N, 30°W. Ship reports and the strength of the surface pressure gradient support wind speeds of 20–25 m s⁻¹ and a fetch length of at least 600 km, with winds directed along the great circle path joining the source point to the *Gilliss* wave-measurement site.

The fetch zone moved eastward at the translation velocity of the cyclone, which was estimated from the sequence of six-hourly surface weather maps to be 20 kt. With *Quadra* located about 130 nautical miles due east from *Gilliss*, one would therefore expect a lag of ~6 h in swell characteristics at *Quadra* with respect to those observed at *Gilliss*. Such a lag is indeed indicated clearly in the energy levels of swell at 0.063 Hz, as shown in Fig. 12, and also at 0.078 Hz, particularly in the time history of mean wave direction. At the highest frequency shown (0.093 Hz), the swell maximum is not well resolved at *Quadra*, but a lag of ~6 h is seen in the reversal in mean wave direction from northerly to southerly. A more thorough directional analysis technique such as described by Long and Hasselmann (1979) should allow further details of the swell from this event to be developed.

6. Concluding discussion

The present state of the art in numerical ocean-wave-specification modeling has been reviewed recently by Cardone and Ross (1978) and by Hasselmann (1978). Basically, several alternative model contexts for wave prediction have been developed in recent years, each reflecting a somewhat different view of the relative importance of the individual physical processes governing wave generation, interaction and dissipation, and of the way in which the nonlinear processes should be parameterized. To date, no single model has been tested extensively enough that it could be reliably applied to wave specification for a wide range of meteorological wind systems and ocean basins. The above referenced reviews have called for objective wave-model intercomparison and validation studies using wave-data sets that include directional spectra and that represent wave environments rather different from the simple regimes (e.g., fetch-limited, homogeneous wind fields, fully developed sea) in which models are developed and tuned. The GATE wave-data set appears to satisfy these requirements. This study demonstrates, however, that such models will have to be applied to a very large domain, including the North Atlantic Ocean to 50°N and at least the subtropical South Atlantic, if the wave environment in the GATE is to be fully modeled. The specification of accurate surface wind fields over the required area represents a considerable challenge, but the extensive GATE meteorological data set should make a suitably accurate wind-field specification possible, at least to about 10°S.

for electronic-system design of the pitch-roll buoy and recording system, and the crews of the U.S. Navy and NOAA aircraft for their contribution to the wind and wave data.

REFERENCES

Cardone, V. J., 1969: Specification of the wind distribution in the marine boundary layer for wave forecasting. Rep. TR-69-1, Geophys. Sci. Lab., New York University, 131 pp. [NTIS AD 702-490].

——, and D. B. Ross, 1978: State-of-the-art wave prediction methods and data requirements. *Ocean Wave Climate*, M. D. Earle and A. Malahoff, Eds., Plenum Press, 61–91.

Cartwright, D. E., J. S. Driver and J. E. Tranter, 1978: Swell waves at St. Helena related to distant storms. *Quart. J. Roy. Meteor. Soc.*, **103**, 655–683.

Garratt, J. R., 1977: Review of drag coefficients over oceans and continents. *Mon. Wea. Rev.*, **105**, 915–929.

Hasselmann, K., 1978: On the application of recent energy balance investigations to numerical wave prediction. *Turbulent Fluxes through the Sea Surface, Wave Dynamics, and Prediction*. A. Favre and K. Hasselmann, Eds., Plenum Press, 531–545.

——, D. B. Ross, P. Müller and W. Sell, 1976: A parametric wave prediction model. *J. Phys. Oceanogr.*, **6**, 200–228.

Kitaigorodskii, S. A., V. P. Krasitsku and M. M. Zaslavskii, 1975: On Phillips' theory of equilibrium range in the spectra of wind-generated gravity waves. *J. Phys. Oceanogr.*, **5**, 410–420.

Krishnamurti, T. N. and R. Krishnamurti, 1978: Surface meteorology over the GATE A-scale. *Deep-Sea Res.*, **26** (Suppl. II, Vol. 2), 29–61.

Long, R. B., and K. Hasselmann, 1979: A variational technique for extracting directional spectra from multi-component wave data. *J. Phys. Oceanogr.*, **9**, 373–381.

Longuet-Higgins, M. S., D. E. Cartwright and N. D. Smith, 1963: Observations of the directional spectrum of sea waves using the motions of a floating buoy. *Ocean Wave Spectra*, National Academy of Sciences, Prentice-Hall, 111–132.

Mitsuyasu, H., 1977: Measurement of the high-frequency spectrum of ocean surface waves. *J. Phys. Oceanogr.*, **7**, 882–891.

——, F. Tasai, T. Suhara, S. Mizuno, M. Okhusu, T. Honda and K. Rikiishi, 1975: Observations of the directional spectrum of ocean waves using a cloverleaf buoy. *J. Phys. Oceanogr.*, **5**, 750–760.

Phillips, O. M., 1958: The equilibrium range in the spectrum of wind generated waves. *J. Fluid Mech.*, **4**, 426–434.

——, 1977: *The Dynamics of the Upper Ocean*, Cambridge University Press, 2nd Ed., 336 pp.

——, and M. L. Banner, 1975: Wave breaking in the presence of wind drift and swell. *J. Fluid Mech.*, **66**, 625–640.

Pierson, W. J., and L. Moskowitz, 1964: A proposed spectral form for fully developed wind seas based on the similarity theory of S. A. Kitaigorodskii. *J. Geophys. Res.*, **69**, 5181–5190.

Report of the U.S. GATE Central Program Workshop, 1977: National Center for Atmospheric Research, Boulder, Colorado, 25 July–12 August, 1977. Published by NCAR. 723 pp.

Resio, D. T., and C. L. Vincent, 1977: A numerical hindcast model for wave spectra on water bodies with irregular shoreline geometry, I: Test of non-dimensional growth rates. Hydraulics Laboratory, U.S. Army Engineer Waterways Experiment Station, Vicksburg, MS, Miscellaneous Pap. H-77-9, 53 pp.

Sadler, J. C., and L. K. Oda, 1978: The synoptic A-scale circulations during the third phase of GATE, 20 August–23 September, 1974. Dept. of Meteorology Rep. UHMET 78-02, University of Hawaii, NSF Grant ATM-7201680.

Snodgrass, F. E., G. W. Groves, K. F. Hasselmann, G. R. Miller, W. H. Munk and W. H. Powers, 1966: Propagation of ocean swell across the Pacific. *Phil. Trans. Roy. Soc. London*, **A259**, pp. 431–497.

Toba, Y., 1978: Stochastic form of the growth of wind waves in a single-parameter representation with physical implications. *J. Phys. Oceanogr.*, **8**, 494–507.

WMO, Geneva, 1976: Progress report on the GATE oceanic boundary layer (C-scale) experiment based on the proceedings of the A-scale oceanographic workshop; Southampton University, England, 16–20 June, 1975. *Preliminary Results*, Vol I, J. P. Woods, Ed., 85 pp.